# Imaging of crystal disorders: calcium pyrophosphate dihydrate crystal deposition disease, calcium hydroxyapatite crystal deposition disease and gout pathophysiology, imaging, and diagnosis

Reijnierse, M.; Schwabl, C.; Klauser, A.

# Imaging of Crystal Disorders:

## Calcium Pyrophosphate Dihydrate Crystal Deposition Disease, Calcium Hydroxyapatite Crystal Deposition Disease and Gout Pathophysiology, Imaging, and Diagnosis

Monique Reijnierse, MD, PhD[a,*], Christoph Schwabl, MD[b], Andrea Klauser, MD, PhD[b]

**KEYWORDS**

• Crystal arthropathy • Calcium pyrophosphate • CPPD • Gout • Hydroxyapatite • Barbotage

**KEY POINTS**

- Including calcifications on radiographic reports is essential, as they may become symptomatic.
- The 3 manifestations of calcium pyrophosphate dihydrate crystal deposition disease: chondrocalcinosis, acute calcium pyrophosphate crystal arthritis, and pyrophosphate arthropathy may overlap or be seen in isolation.
- In crystal deposition diseases a cascade of reactions leading to joint inflammation can be age related, triggered by a trauma or disease, and result in sometimes rapid joint destruction.
- Ultrasound-guided barbotage procedure is straightforward and accelerates the natural course of hydroxyapatite crystal deposition disease.
- Dual-energy computed tomography is rapid, noninvasive, and enables diagnosis and follow-up of gout, in multiple joints on a single scan without the use of contrast agents.

## INTRODUCTION

In the elderly population a variety of calcifications and crystal depositions can be appreciated on conventional imaging. These might be asymptomatic but may become symptomatic in time and deserve to be mentioned in the radiological report. The clinical presentation of crystal deposition diseases is variable and diagnosis might be challenging.[1,2] The purpose of this review article is to explain the disease spectrum and pathophysiology of calcium pyrophosphate dihydrate crystal deposition disease (CPPD), hydroxyapatite crystal deposition disease (HADD), and gout; to describe imaging findings; and to learn about differential diagnoses, choice of imaging modalities, and possible clinical consequences. Pearls and pitfalls relevant to point of care are provided.

## CALCIUM PYROPHOSPHATE DIHYDRATE CRYSTAL DEPOSITION DISEASE

### *Introduction*

CPPD is caused by the deposition of calcium pyrophosphate (CPP) crystals predominantly in, but also around, joints, and it is common in elderly persons.[1,2] There is no gender difference. Its prevalence increases with age: using radiographic knee chondrocalcinosis as diagnostic criterion, it is uncommon in those younger than 55 years and

[a] Department of Radiology, Leiden University Medical Center, PO Box 9600, Leiden, 2300 RC, the Netherlands;
[b] Department of Radiology, Medical University Innsbruck, Anichstrasse 35 A-6020, Innsbruck, Austria
* Corresponding author.
*E-mail address:* m.reijnierse@lumc.nl

Radiol Clin N Am 60 (2022) 641–656
https://doi.org/10.1016/j.rcl.2022.03.007

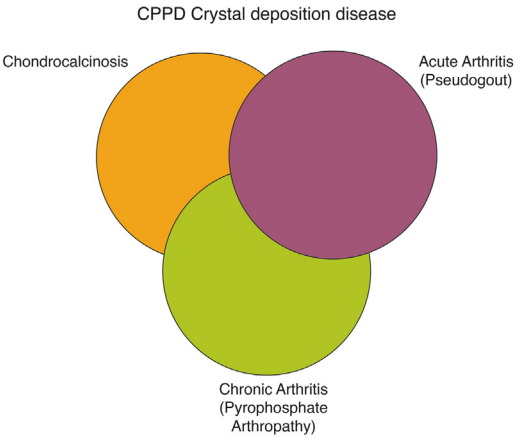


**Fig. 1.** All 3 CPPD stages may be present in one patient. Diagnosis may become more difficult when 2 or only 1 stage is seen. (*Adapted from* Resnick D. Calcium pyrophosphate dihydrate crystal deposition disease. In: Diagnosis of bone and joint disorders, 4th edition (Articular diseases, vol 1). Philadelphia: WB Saunders; 2002. p.1560-1618.)

increases to 20% to 30% in those older than 80 years.[1,3–5] The mechanism of CPP crystal accumulation in cartilage is unknown. The theory is that it is secondary to cartilage damage: age related, posttraumatic, or disease induced.[1] There is a positive association with osteoarthritis; however, CCPD deposition is not considered a risk factor for progressive cartilage loss.[5] Less commonly genetic or various metabolic disorders such as hereditary hemochromatosis, primary hyperparathyroidism, and hypomagnesemia are the cause,[1,6] and this should be considered in case of CPP deposition when younger than 55 years or excessive polyarticular involvement.[5] Its clinical expression is variable; patients may present with chondrocalcinosis, acute CPP crystal arthritis (also called pseudogout), or pyrophosphate arthropathy, as a result of chronic CPP arthritis[7,8] (**Fig. 1**). There is no medical treatment of CPPD, and in case of progressive degenerative changes, joint replacement might be an option.[1] Treatment of acute or chronic arthritis in CPPD is based on expert opinion and evidence based on treatment of gout. A recent review article showed that the administration of nonsteroidal antiinflammatory drugs (NSAIDs), colchicine, and corticosteroids has not been evaluated by randomized controlled trials.[9]

- Chondrocalcinosis: the asymptomatic form of this crystal arthropathy is probably the most common with absence of symptoms in at least 10% to 20%[1] (**Fig. 2**).

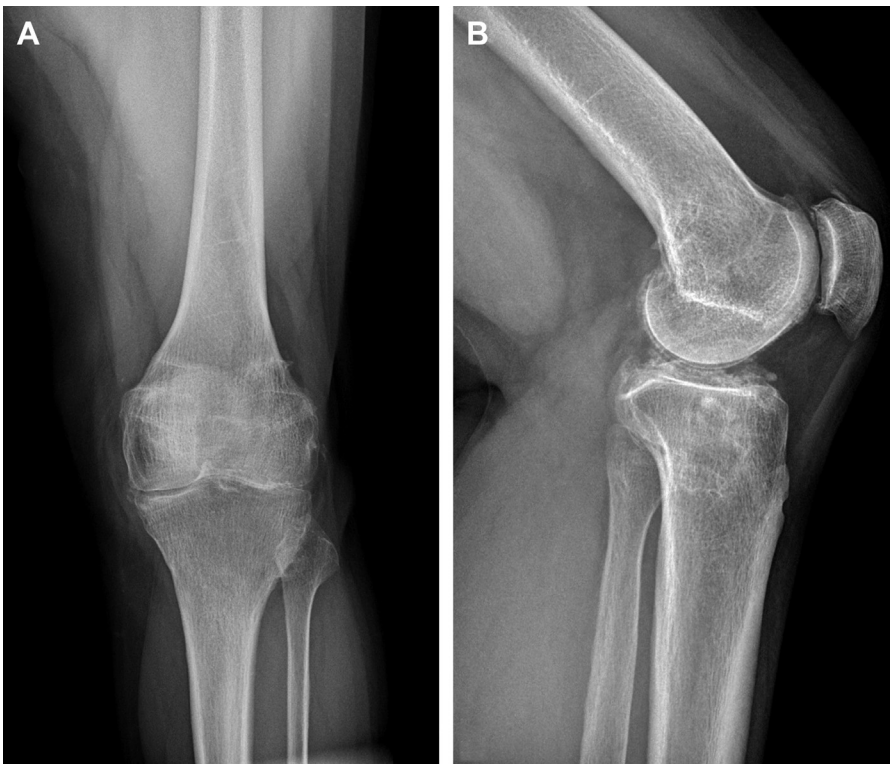


**Fig. 2.** Granular calcifications of hyaline cartilage parallel to the cortical bone in femorotibial and patellofemoral joints A, B. Fibrocartilage calcifications in the menisci and proximal patella enthesopathy.B

- Acute CPP crystal arthritis (pseudogout syndrome): CPPD was first recognized as a source of acute crystal-induced peripheral-joint inflammation. Most cases develop spontaneously, but there are situations that trigger arthritis, for instance joint trauma, medical illness, surgery, or a blood transfusion.[2,8] The European League Against Rheumatism has made recommendations for the diagnosis of CPPD based on rapid development of inflammatory symptoms, the location of arthritis (knee, shoulders, wrist), age of the patient (>65 years), imaging findings, and absence of another disease (eg, rheumatoid arthritis and septic arthritis).[8] The theory of pathogenesis of acute arthritis and synovitis in CPPD is shown in the drawing of **Fig. 3**A, B. The shedding of CPP crystals into the joint is key in this process. This acute onset of CPP arthritis is self-limiting.[8]
- Pyrophosphate arthropathy: the clinical presentation often simulates osteoarthritis. CPPD flares may occur, and a chronic and progressive form of arthritis develops. Its presence is often bilateral and symmetric. Preferential locations include the knee, hip, metacarpophalangeal joints, elbow, ankle, wrist, and glenohumeral joints.[1]

### *Imaging Findings and Pathology*

- Radiography

Chondrocalcinosis is most frequently seen in knees, wrists, symphysis pubis, elbows, and hips.[2] The intraarticular deposition of CPP crystals is almost exclusively seen into articular hyaline cartilage and fibrocartilage and is the most common cause of chondrocalcinosis (see **Fig. 3**). Examples of fibrocartilage calcifications include knee menisci, symphysis pubis, triangular cartilage of the wrist, annulus fibrosis of the intervertebral disc, and labra of hip and shoulder. However, not all calcifications are identified on radiographs; this can be based on low density of the calcifications or an already severely deranged joint at presentation.[1,10] Calcifications can also be seen in the synovial membrane (eg, the knee, wrist, metacarpophalangeal, and metatarsophalangeal [MTP] joints) and the joint capsules. In addition, periarticular calcifications in tendons, bursae, and ligaments can be observed, mimicking hydroxyapatite deposition.[1,2,11] In the spine all ligaments may be affected. Periodontoid deposition is called the crowned dens syndrome.

The term pyrophosphate arthropathy is used for the structural joint changes in CPPD (see **Fig. 3**). Characteristics include the following:

- Cystic degeneration and sclerosis (no erosions)
- Fragmentation of bone and cartilage
- Debris in synovial membrane
- Ultrasonography (US)

  US can show synovitis and can sensitively show CPP deposits in cartilage, with a typical appearance of hypoechoic (cartilage) and echoic (CPPD) layers, being part of the EULAR criteria.[8]
- Computed tomography (CT)

  CT technique is able to accurately show calcifications but is rarely used additional for diagnosis or evaluation of a painful joint.[1]
- MR Imaging

The value of MR imaging is limited in the diagnosis of CPPD. The calcifications are low of signal intensity on all MR sequences and difficult to identify especially in ligaments, and correlation with conventional radiographs is necessary.[12] In cartilage, depositions can be recognized.[13]

### *Diagnostic Criteria*

- The 3 manifestations of CPPD may overlap (see **Fig. 1**). Knowledge of the characteristics of CPPD arthropathy ensures an accurate diagnosis.[2,8,9]

### *Differential Diagnosis*

- Gout (see **Fig. 3**C)[8,14]
- Septic arthritis
- Charcot arthropathy
- Synovial osteochondromatosis
- Degenerative joint disease
- HADD

## CALCIUM HYDROXYAPATITE CRYSTAL DEPOSITION DISEASE

### *Introduction*

Deposition of calcium HA crystals is predominantly periarticular in tendons and bursae but also in ligaments being the source of inflammatory periarthritis, such as bursitis or tendinitis.[15] HADD is usually monoarticular; the shoulder is most frequently involved, affecting people between the age of 40 and 60 years.[1] The second most common site is the hip followed by elbow, wrist, hand, and knee, but any joint can be affected, including the cervical and lumbar spine.[11,12] Intraarticular depositions can lead to arthritis or destructive arthropathy[16,17] (**Fig. 4**). This arthropathy is more frequent in women in an older age group (50–90 years) and bilateral in 65% of cases.[17] Milwaukee shoulder syndrome is

associated with rotator cuff pathology, and arthropathy in other joints, especially the knee, is reported, typically unicompartmental[15,16] (**Fig. 5**). The differential diagnosis includes CPPD arthropathy, neuropathic arthropathy, and infection.

The cause and pathogenesis of calcium HA deposition is unknown. Several theories in the past included tendon degeneration, hypoxia, (repetitive) trauma, and aging.[15] In case of bilateral and polyarticular presence, a genetic, neurologic, or metabolic origin can be considered.[15] Most calcifications are incidental findings, and other pathology should be excluded before focusing on the calcific deposit as the source of complaints.

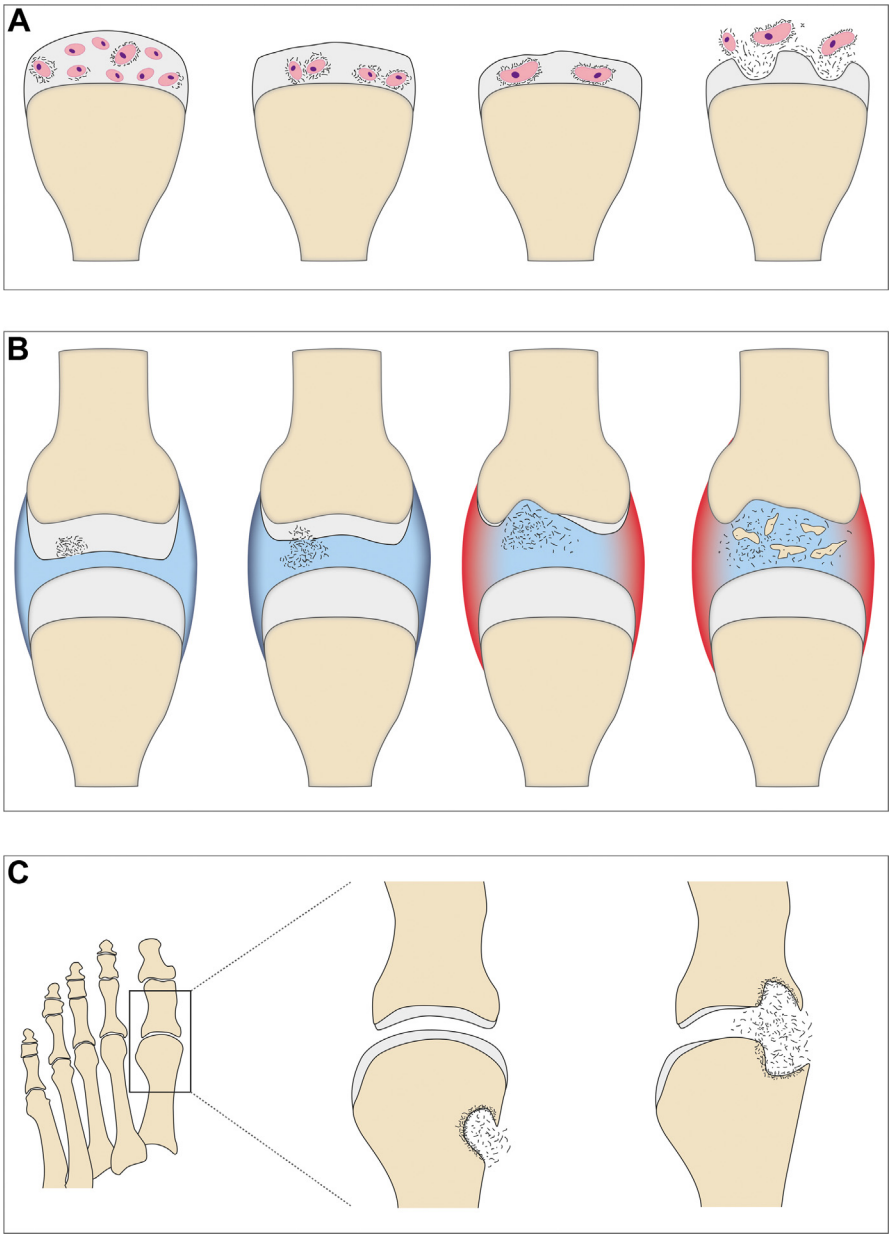


**Fig. 3.** Pathogenesis of CPPD (*A*, *B*) and gout (*C*). (*A*) Acute CPPD attack hypothesis. Crystal deposits around chondrocytes (chondrocalcinosis) lead to cell death, cartilage loss, and deposit coalescence. Crystal shedding results in arthritis. (*B*) Pyrophosphate arthropathy pathogenesis. Cartilage loss and crystal shedding with synovial depositions result in synovitis. In time degenerative cysts and progressive cartilage and bone destruction is seen. (*C*) Gout. MTP1 is preserved; MSU crystals erode the bone in intra- and extraarticular eccentric locations, leading to overhanging margins. (*Adapted from* Resnick D. Gouty arthritis. In: Diagnosis of bone and joint disorders, 4th edition (Articular diseases, vol 1). Philadelphia: WB Saunders; 2002. P.1519-1559.)

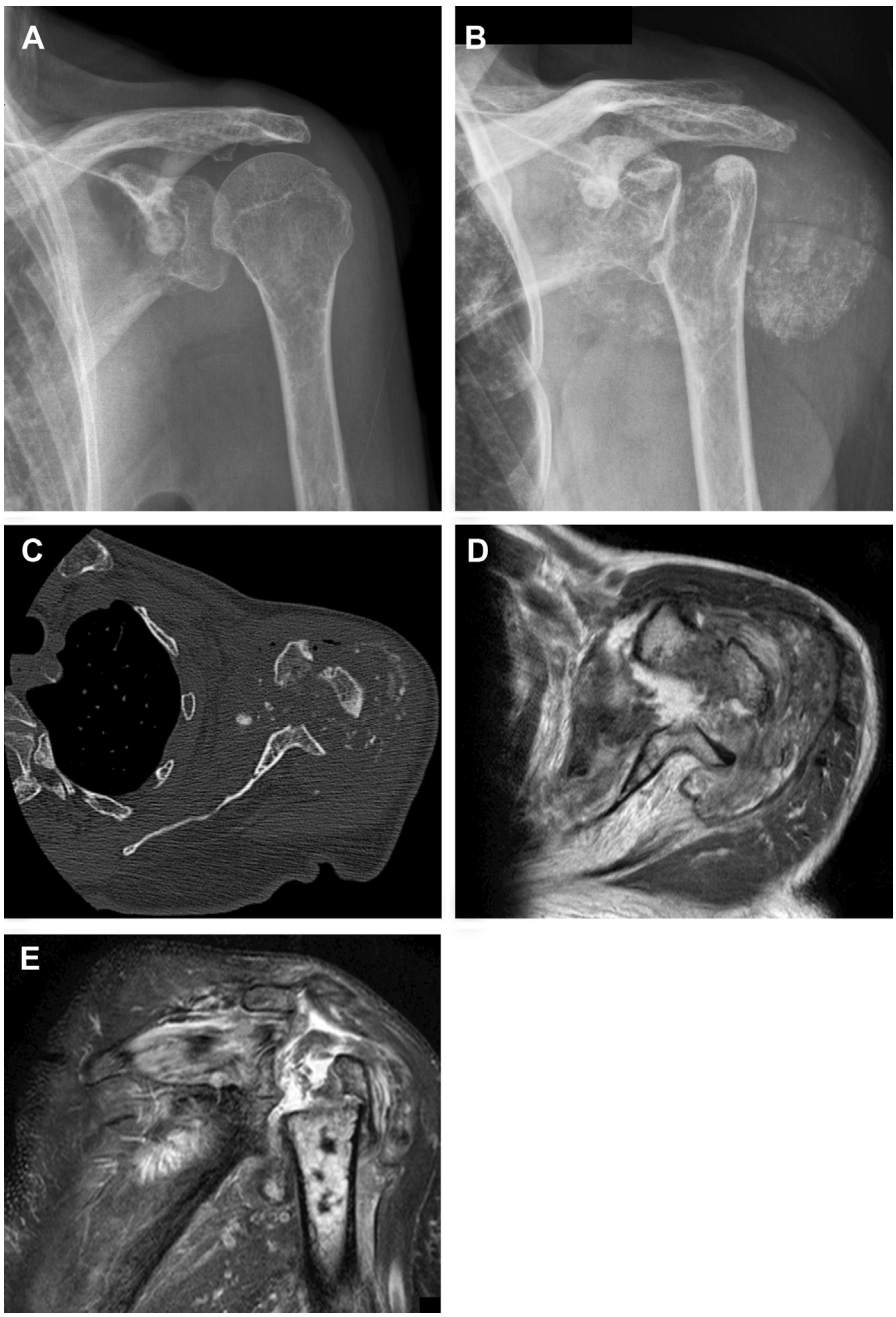


**Fig. 4.** Milwaukee shoulder syndrome. Posttraumatic left shoulder (*A*) of an 80-year-old woman without fracture and preexisting rotator cuff pathology. After 6 weeks (*B*) complete destruction of the humeral head and a large soft tissue mass with multiple bony fragments is seen. Axial CT image (*C*), T1TSE (*D*), and coronal T2fatsat MR images (*E*) show complete humeral head destruction with several bony fragments, surrounded by fluid and debris, extending into the subacromial bursa secondary to rotator cuff pathology.


**Fig. 5.** Arthropathy of the right knee in same patient as **Fig. 4**. Intraarticular fluid, valgus deviation, and large lateral tibia plateau impression with demarcated sclerosis A. Multiple intraarticular bony fragments are present A, B.

Calcific tendinitis of the rotator cuff has a reported prevalence of 6.8% to 54% in patients with shoulder pain.[18–20] It is considered a self-limiting disease with low-grade pain, and treatment is preferably conservative including physical therapy and NSAIDs.[20] However, symptoms can be severe and long-lasting, and several treatments have been initiated including subacromial corticosteroid injections, high-energy extracorporeal shock wave therapy, barbotage, and surgery.[20,21] Barbotage and subacromial injections are among the most frequently applied treatments in calcific tendinitis of the rotator cuff.[22,23]

## *Imaging Findings and Pathology*

- Radiographs

Three stages of calcific deposits have been described: a formative, resting, and resorptive phase.[18,19] Different types of calcific deposits can be classified according to Gärtner and correlated to these different phases.[24]

- Type I calcifications have a sharp border and a dense structure
- Type II calcifications either have a sharp border and inhomogeneous structure or a vague border and a homogenous structure
- Type III calcifications have a vague border, and are more or less transparent, with a cloudy appearance.

In the phase of resorption, calcifications can migrate into the soft tissues: the tendon, bursa, joint, but also the bone. On radiographs faint small calcifications can be appreciated in the area of the bursa (**Fig. 6**). This chemical bursitis can be extremely painful and important to recognize. A calcification can also migrate into the bone, leading to cortical erosions (**Fig. 7**). In the resorptive phase the radiograph might not show calcific deposits, and other imaging modalities such as ultrasound and MR imaging might be of help.[12]

- Ultrasonography

On US the calcifications will have a different appearance based on their content. A dense type I calcification will show acoustic shadowing, whereas a type II can be more clearly visualized with a hyperechoic margin (**Fig. 8**A). During a barbotage procedure the calcific deposit can show a change in echogenicity because crystals are washed out (**Fig. 8**D, E) and the posterior border can become visible.

US can visualize radiographic undetected calcifications because of size or density and determine their exact location (see **Fig. 6**). In addition, US-


**Fig. 6.** Large unsharply defined calcification (type II) in the supraspinatus tendon (*A*). Two days after barbotage the patient presented with severe shoulder pain. The calcification (*B*) shows resorption and fragmentation on ultrasound present in SSP tendon (*C*) and bursa (*D*).

Doppler will show inflammation in bursae, tendons and joints (see **Fig. 8**A). Moreover, US is the ideal tool for an accurate bursal injection and barbotage procedure (**Fig. 8**; **Figs. 9** and **10**).

Barbotage treatment is invasive, needs coordinating skills, and is time consuming. It can be painful during and after the intervention but is reported to accelerate the natural course of HADD in randomized controlled trials.[20,22,23]

- CT and MR imaging are less frequently used in HADD

However, in unclear diagnosis these modalities might be of help: CT in detecting small

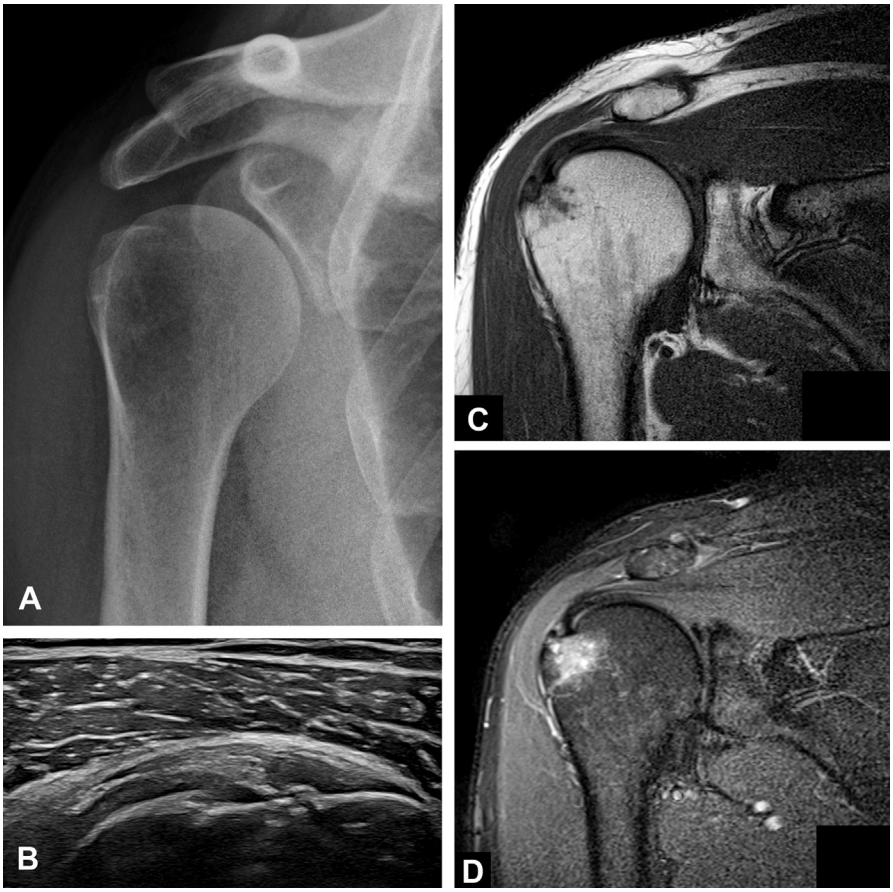


**Fig. 7.** Unremarkable radiograph (*A*). Ultrasound (*B*) of the supraspinatus insertion shows multiple small calcifications and a cortical break with intraosseous extension of calcifications. No bursitis. Coronal T1TSE (*C*) and T2fatsat MR images (*D*) show SSP enthesitis and several subchondral cysts and extensive bone marrow edema at the footprint.

calcifications, intraosseous erosion, and for example, evaluation of deposits in the spine. On MR imaging calcifications are less evident; however, soft tissue involvement and bone marrow edema can be detected (see **Fig. 7**).[12,25]

## GOUT

### *Introduction*

With a prevalence of approximately 1% to 7%, gout has become a major cause for musculoskeletal pain and arthritis.[26–29] Its prevalence and incidence seem to be increasing across the globe, especially in industrialized nations and in male population.[30–34] Sustained elevation of serum urate levels results in a deposition of monosodium urate (MSU) especially in or around joints, which can lead to formation of tophi and joint damage.[35] MSU deposits may be intratendinous, peritendinous, or at the enthesis as well.[36–39] Peripherally located structures and structures of the lower limbs are especially frequently affected by gout, with a predilection for the first MTP joint; this is classically described as podagra and is reported in up to 80% of untreated patients.[40] A recent survey showed that gout presented with single joint involvement in more than 90% of patients, whereas fewer than 1% of patients presented with gout affecting more than 4 joints.[41] Clinical presentation typically consists of recurrent episodes of acute arthritis with a rapid onset of severe pain, swelling, and erythema. Gout further has a strong association with cardiovascular diseases.[42] Elevation of serum urate levels can have several causes: exogenous, due to excessive intake of purines (eg, meat, seafood, alcohol), or endogenous, for example, cell lysis during chemotherapy or myeloproliferative disorders.[43] Insufficient uric acid

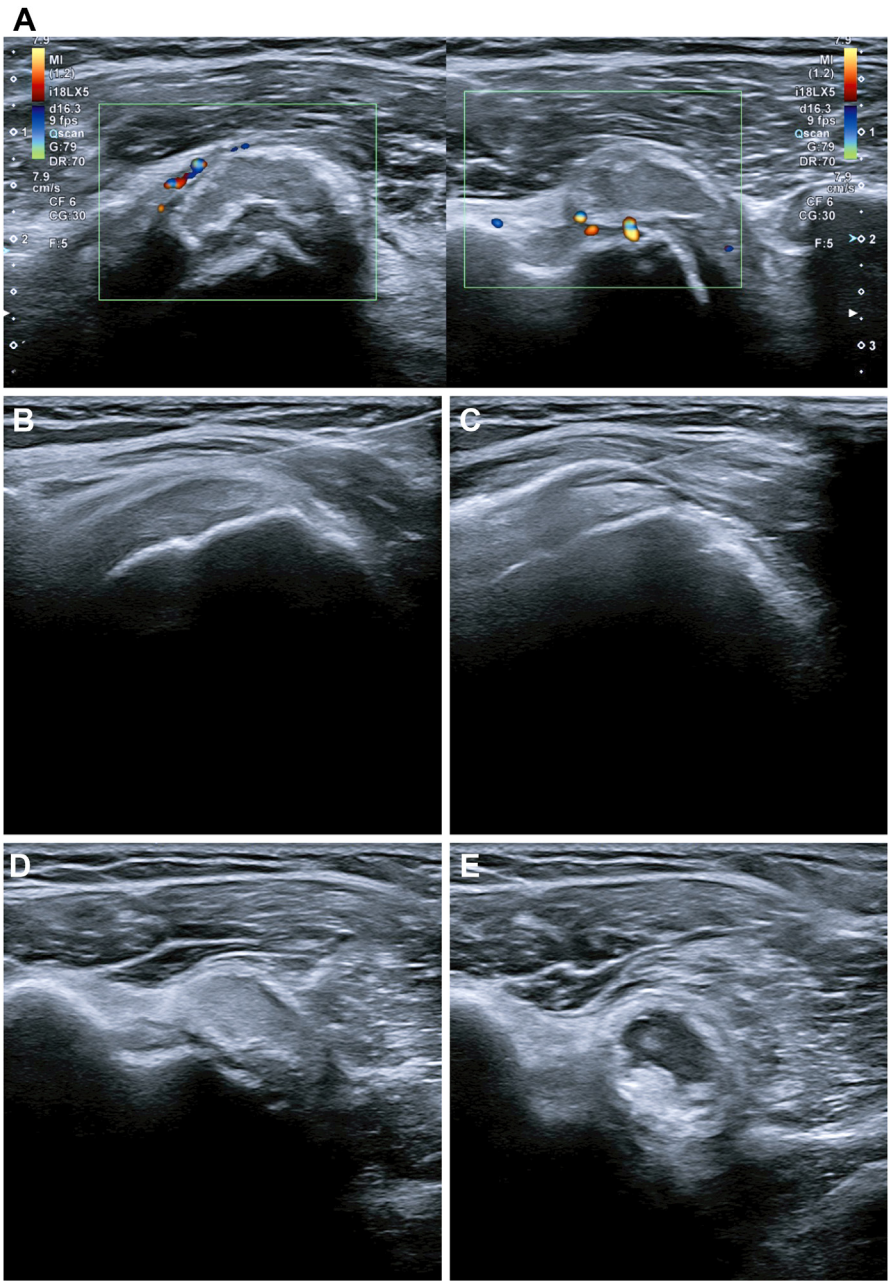


**Fig. 8.** Large subscapularis calcification with a hyperechoic demarcated rim and less hyperechoic content, surrounding hyperemia in longitudinal (*left*) and axial view (*right*) (*A*). Bursal injection of 1cc corticosteroid (40 mg/ml) and 4cc bupivacaine 5 mg/ml (*B*, *C*). Lavage of the calcification (*D*), with hypoechoic saline (*E*).

clearance also plays a major role in the development of elevated serum urate, either from chronic kidney disease, drug interactions, or genetic predispositions.[44] Demonstrating MSU crystals in joint fluid or in a tophus by puncture with polarizing microscopy is still the gold standard for the diagnosis of gout[45] (**Fig. 11**). However, this is invasive with potential contraindications, leading to the increasing role of US and dual-energy computed tomography (DECT) in gout detection.[46–48] Both US and DECT are included in the new 2020 American College of Rheumatology classification

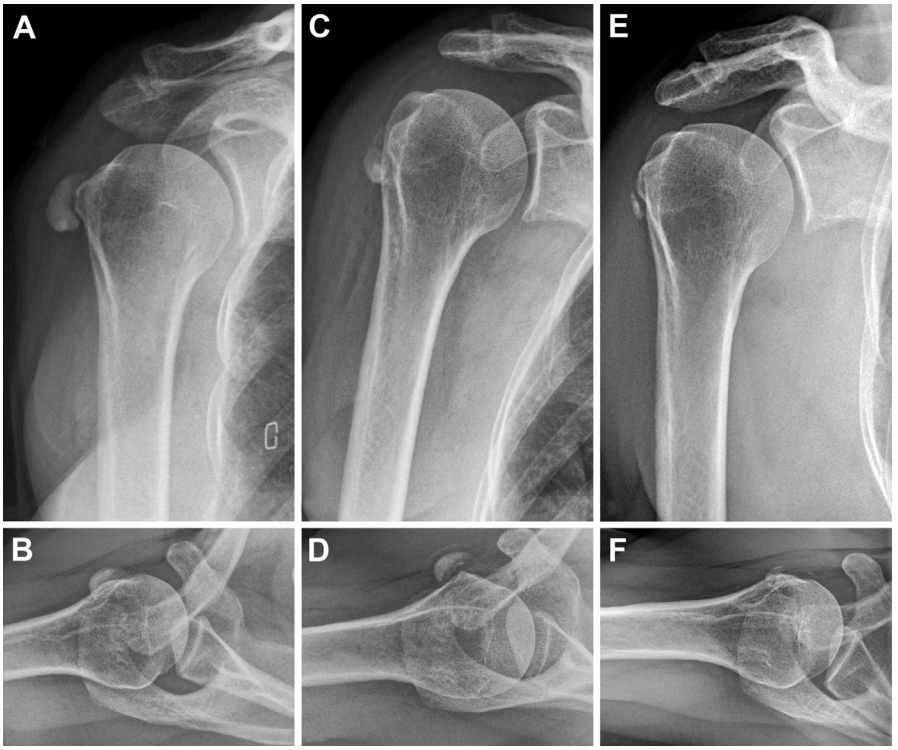


**Fig. 9.** Anteroposterior and axial views of the right shoulder, before (*A*, *B*), after (*C*, *D*), and 6 weks after barbotage (*E*, *F*). The large calcification in the subscapularis tendon has decreased in size.

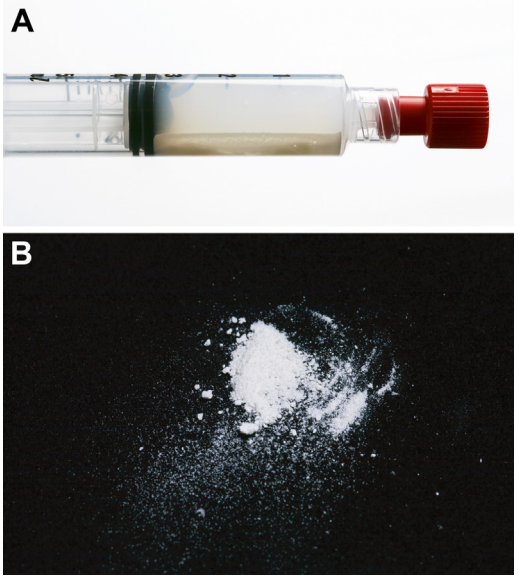


**Fig. 10.** Syringe with saline and calcific deposits layered at the bottom (*A*). Dried amorphous white calcifications (*B*).

criteria, along with radiographs, elevated serum urate levels, clinical evidence of tophus, and MSU crystals in synovial fluid.

### *Imaging Findings*

- Radiography

Radiographs are indicated to search for imaging evidence of MSU crystal deposition but have limited value for the diagnosis of gout flare. The radiographic changes take several years to develop, thus helpful in supporting diagnosis of chronic gout. In patients with 4 years duration of disease, sensitivity and specificity for erosions were 0.12 and 0.96.[49] Radiographic manifestations are classified into early, intermediate, and late stage.

  - Early findings are nonspecific soft-tissue swelling in the affected joint secondary to synovitis, capsular distension, and periarticular soft tissue edema. Fine lacy periosteal reaction may be observed secondary to urate crystals in adjacent soft tissue.
  - Intermediate-stage features include faint calcification of affected soft tissues, intracortical erosions and irregularity, and osteochondral compression or cupping. The joint space is preserved until late in the disease.

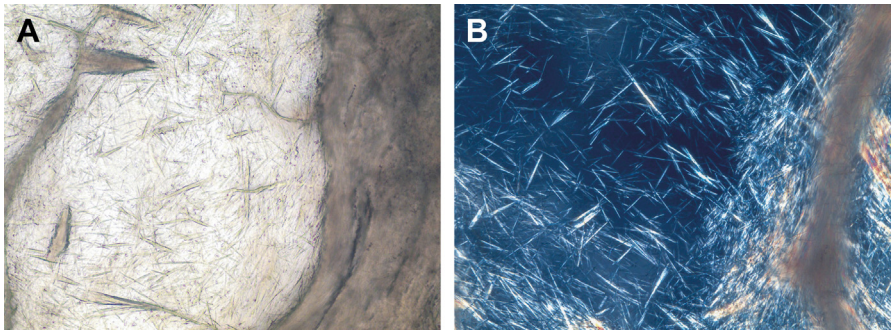


**Fig. 11.** Needle-shaped crystals of monosodium urate (*A*), showing strongly birefringent crystals on polarization (*B*) Zeiss Axioskop and Leica DM2000 light microscope: 400x enlargement.

- Late stage is characterized by well-defined juxta-articular erosions with sclerotic rims and overhanging margins. Progressive erosions and intraarticular deposits may result in tapering deformities of the shafts, subluxation, and mutilating arthritis. Progressive joint space narrowing with secondary degenerative changes is a late manifestation. Rarely, ankylosis may occur. Appositional bone deposition may cause apparent expansion of bone ends with a bulbous appearance.[50,51]

- Ultrasonography

US is an ideal first-line examination technique for suspected gout. MSU deposits can have several different appearances, including the "double contour sign" (DC-sign), "snow storm sign," and delineation of tophi.[52]

- DC-sign

An abnormal hyperechoic band over the superficial margin on the hypoechoic articular hyaline cartilage, which may be homogeneous or inhomogeneous, irregular or regular, and continuous or intermittent. There may be posterior acoustic shadowing, depending on both the amount and density of the MSU deposits.[53] The thickness of the DC sign should be similar to the cortex; however, in early stages it may be thinner (**Fig. 12**A, B).

- Snow-storm sign and tophi: hyperechoic microtophi appearing as white spots within the fluid collection generate the typical snow storm appearance. Larger, dense aggregates develop into hypoechoic to hyperechoic (mainly chronic tophi) inhomogeneous tophi, with a cloudy appearance and a hypoechoic or anechoic rim[54,55] (**Fig. 13**).

Although those appearances are very specific for gout, data regarding specificity and sensitivity are highly variable depending the examined region. Although regions that can be easily assessed by US such as the MTP1 joint show great data, regions such as the hand and wrist show poor gout detection, as these joints are less accessible. In these joints US showed a sensitivity of 70.1% (extraarticular: 42.5%, $P < .001$; intraarticular: 80.3%, $P = .14$) and a specificity of 51%.[56]

- MR Imaging

On MR imaging, tophi can be seen as amorphous or nodular regions of low-intensity signal

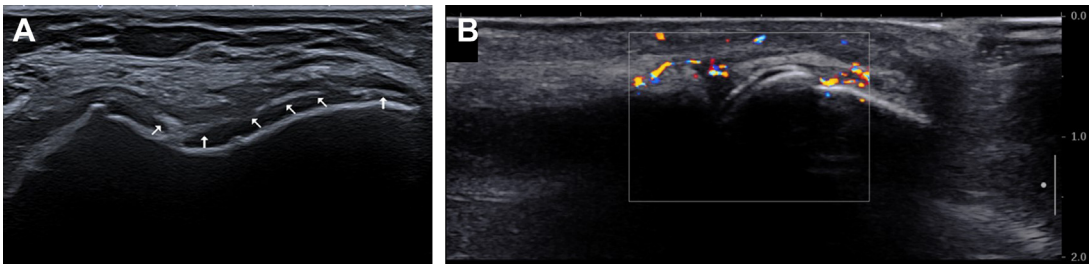


**Fig. 12.** (*A*) Double contour (DC) sign (*arrows*) in an axial US scan of the knee in a patient with gouty arthritis, with a hyperechoic band over the articular cartilage (hypoechoic) of the condyles. (*B*) DC sign in a sagittal US scan of an MCP joint with surrounding hypervascularization.

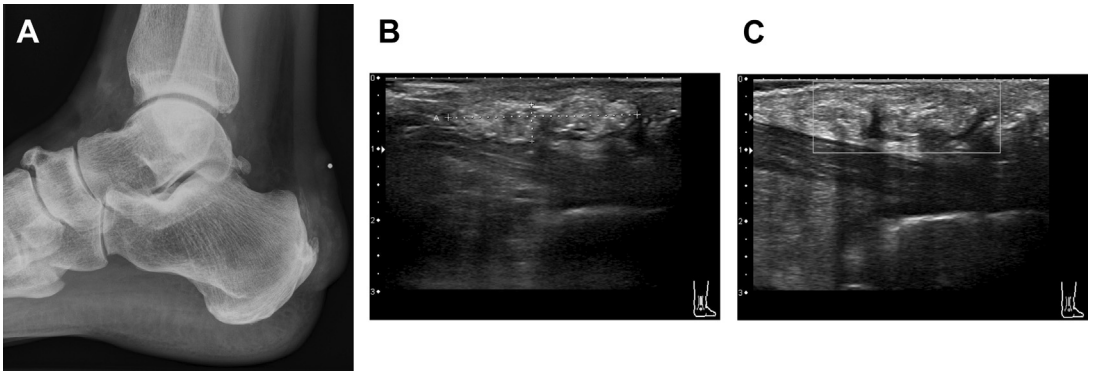


**Fig. 13.** Large gout tophus at the level of the Achilles tendon insertion on lateral radiograph of the right ankle (*A*). Longitudinal ultrasound (*B*) shows an inhomogeneous hyperechoic mass with a surrounding hypoechoic rim, without hyperemia (*C*).


**Fig. 14.** Left foot dorsoplantar (*A*) and $^{3}/_{4}$ view (*B*) show erosive destruction in the tarsus and MTP joints. Sagittal MR images, T1TSE (*C*), T2TSE fatsat (*D*), and T1TSE fatsat after intravenous contrast (*E*) show multiple sharply delineated erosions in the tarsal bones. The moderately high T2 content shows a peripheral zone of enhancement. Absence of intraosseous edema. DECT, 3D-formatted (*F*), axial subtracted images in bone (*G*) and soft tissue (*H*) setting. Color-coded green MSU deposits in the erosions. 3D, 3-dimensional.

on T1-weighted images, variable intensity on T2-weighted images and with variable enhancement after intravenous contrast media. Other MR imaging features of gout are synovial pannus, joint effusions, and soft-tissue edema.[57,58] A particular advantage of MR imaging is the ability to assess bone involvement in detail, being more sensitive than both CT and US in detecting bone erosion in patients with gout. A main disadvantage is that MSU crystals cannot be directly observed by MR imaging, leading to poor specificity[59] (**Fig. 14**).

- Dual-energy Computed Tomography

The unique chemical composition of uric acid precipitates results in a distinct radiographic attenuation when compared with other materials, and this results in characteristic patterns of CT numbers at high versus low kilovolts (kV), allowing imaging software to differentiate MSU from other materials.[48,60] The effectiveness of noncontrast DECT has been proved in several studies,[47,56,61–65] and DECT is increasingly being used for the diagnosis and follow-up of gout, with a reported sensitivity of 78% to 100% and specificity of 89% to 100%[66] (**Fig. 15**). DECT scanning is rapid and noninvasive and enables multiple joints to be imaged on a single scan without the use of contrast agents.[67] Data are acquired at 80 and 140 kV with a plot of the attenuation of each voxel at 80 kV (y-axis) against attenuation at 140 kV (x-axis). The pixels containing calcium and monosodium urate can be separated and presented as a color image for easy identification. Although the color coding can vary across manufacturers, the most common software color codes are green for MSU deposits, lavender for cortical bone, and pink for trabecular bone. These color-coded images are displayed as an overlay on either 2-dimensional conventional gray-scale CT images or as 3-dimensional volume-rendered images[68] (see **Figs. 14** and **15**; **Fig. 16**). DECT can therefore provide color-coded information about the composition of certain materials, including urate, calcium pyrophosphate (CPPD), and hydroxyapatite (HADD). Mallinson and colleagues concluded that nail bed deposits, submillimeter deposits, skin deposits, and deposits obscured by motion, beam hardening, and vascular artifacts

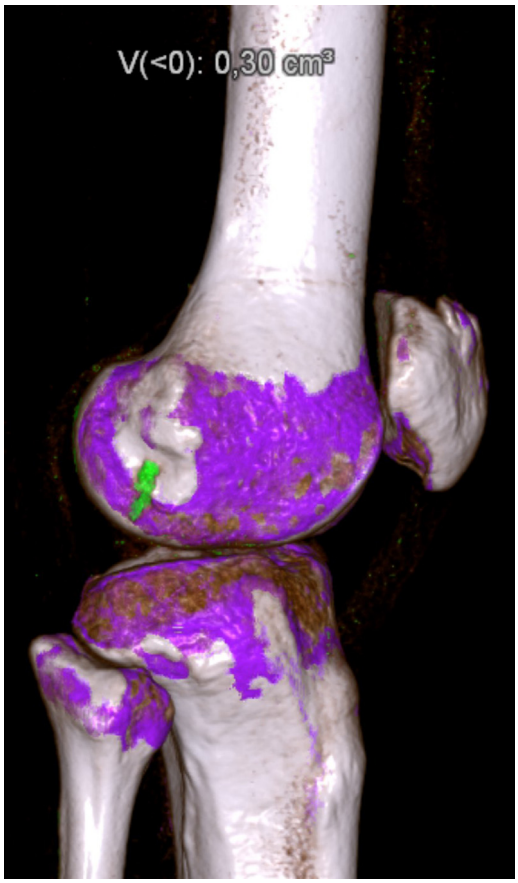


**Fig. 15.** MSU deposits in a 3D reconstructed DECT of the knee, showing color-coded green MSU deposit in the lateral condyle.


**Fig. 16.** Coronal DECT of the hand shows color-coded green MSU deposits in the second MCP joint, as well as in the lateral aspect of the os triquetrum.

should not be classified as positive findings, and they are especially dependent on the postprocessing protocols used.[69] Park and colleagues concluded that setting the minimum attenuation to a higher value of 150 Hounsfield units in their study reduced the frequency of artifacts and that adding a tin filter to DECT greatly reduced their occurrence.[70] A prospective blinded randomized study by Choi and colleagues[71] showed 84% sensitivity and 93% specificity for detection of MSU deposits by DECT in the lower extremities, as well as wrists and hands. The role of DECT has also been shown by Hu and colleagues[61] reporting a high sensitivity and specificity of 75.2% and 92.7% of DECT for the detection of gouty arthritis in upper and lower extremities. In recent studies a modified postprocessing protocol with lowering of the threshold of attenuation from 150 HU to 120 HU and keeping the kilovoltage settings constant showed promising results.[56,64,72] DECT may also demonstrate cardiovascular MSU deposits, which might have implications for patients who are at risk of cardiovascular disease.[73,74]

## SUMMARY

Crystal arthropathies are a group of joint disorders due to deposition of crystals in and around joints, which lead to joint destruction and soft tissue masses. Clinical presentation is variable and diagnosis might be challenging. Therefore, first-line imaging of ultrasound in accessible joints is recommended to assess crystal arthropathies; however, DECT is a useful adjunct to differentiate gout from CPPD.

## CLINICS CARE POINTS

- Aging is the main risk factor for CPPD crystal deposition disease.
- CPP crystals almost exclusively deposit into articular fibrocartilage and hyaline cartilage, the most common cause of chondrocalcinosis.
- Calcifications need to be part of the radiological report, as they may become symptomatic.
- Absence of crystal deposit detection on radiographs does not exclude the diagnosis of CPPD, gout, or HADD.
- Rapid joint destruction without visible calcifications should raise the diagnosis of CPPD.
- Barbotage is an effective method to accelerate the natural course of HADD.

## DISCLOSURE

The authors have nothing to disclose.

## REFERENCES


1. Steinbach LS. Calcium pyrophosphate dihydrate and calcium hydroxyapatite crystal deposition disease: imaging perspectives. Radiol Clin North Am 2004;42:185–205.
2. Resnick D. Calcium hydroxyapatite crystal deposition disease. In: Diagnosis of bone and joint disorders. 4th edition. Articular diseases, vol 1. Philadelphia (PA): WB Saunders; 2002. p. 1619–1657.
3. Felson DT, Anderson JJ, Naimark A, et al. The prevalence of chondrocalcinosis in the elderly and its association with knee osteoarthritis: the Framingham Study. J Rheumatol 1989;16:1241–5.
4. Neame RL, Carr AJ, Muir K, et al. UK community prevalence of knee chondrocalcinosis: evidence that correlation with osteoarthritis is through a shared association with osteophyte. Ann Rheum Dis 2003;62:513–8.
5. Richette P, Bardin T, Doherty M. An update on the epidemiology of calcium pyrophosphate dihydrate crystal deposition disease. Rheumatology 2009; 48(7):711–5.
6. Huaux JP, Geubel A, Koch MC, et al. The arthritis of hemochromatosis. A review of 25 cases with special reference to chondrocalcinosis, and a comparison with patients with primary hyperparathyroidism and controls. Clin Rheumatol 1986;5(3):317–24.
7. Ea H-K, Lioté F. Diagnosis and clinical manifestations of calcium pyrophosphate and basic calcium phosphate crystal deposition diseases. Rheum Dis Clin North Am 2014;40:207–29.
8. Zhang W, Doherty M, Bardin T, et al. European League Against Rheumatism recommendations for calcium pyrophosphate deposition. Part I: terminology and diagnosis. Ann Rheum Dis 2011;70:563–70.
9. Parperis K, Papachristodoulou E, Kakoullis L, et al. Management of calcium pyrophosphate crystal deposition disease: A systematic review. Semin Arthritis Rheum 2021;51(1):84–94.
10. Resnick D, Utsinger PD. The wrist arthropathy of "pseudogout" occurring with and without chondrocalcinosis. Radiology 1974;113:633–41.
11. Jacques T, Paul M, Badr S, et al. Conventional radiology in crystal arthritis gout, calcium pyrophosphate deposition, and basic calcium phosphate crystals. Radiol Clin North Am 2017;55:967–84.
12. Reijnierse M. Radiographic/MR imaging correlation of paravertebral ossifications in ligaments and bony vertebral outgrowths: anatomy, early detection, and clinical impact. Magn Reson Imaging Clin N Am 2019;27(4):641–59.

13. Beltran J, Marty-Default E, Bencardino J, et al. Chondrocalcinosis of the hyaline cartilage of the knee: MRI manifestations. Skeletal Radiol 1998;27:369–74.
14. Towiwat P, Doyle AJ, Gamble GD, et al. Urate crystal deposition and bone erosion in gout: "inside-out" or "outside-in"? A dual-energy computed tomography study. Arthritis Res Ther 2016;18(1):208–2014.
15. Resnick D. Calcium hydroxyapatite crystal deposition disease. In: Diagnosis of bone and joint disorders, 4th edition (Articular diseases, vol 1). Philadelphia: WB Saunders; 2002. p. 1619–57.
16. Halverson PB, Carrera GF, McCarty DJ. Milwaukee shoulder syndrome. Fifteen additional cases and a description of contributing factors. Arch Intern Med 1990;150(3):677–82.
17. McCarthy DJ, Swanson AB, Ehrhart RG. Haemorraghic rupture of the shoulder. J Rheumatol 1994;21(6):1134–7.
18. Uhthoff HK, Loehr JW. Calcific tendinopathy of the rotator cuff : pathogenesis, diagnosis and management. J Am Acad Orthop Surg 1997;5(4):183191.
19. Speed CA, Hazleman BL. Calcific tendinitis of the shoulder. N Engl J Med 1999;340:1582–4.
20. de Witte PB, Selten JW, Navas A, et al. Calcific tendinitis of the rotator cuff: a randomized controlled trial of ultrasound-guided needling and lavage versus subacromial corticosteroids. Am J Sports Med 2013;41(7):1665–73.
21. Louwerens JKG, Sierevelt I, Kramer ET, et al. Comparing ultrasound-guided needling combined with a subacromial corticosteroid injection versus high-energy extracorporeal shockwave therapy for calcific tendinitis of the rotator cuff: a randomized controlled trial. Arthroscopy 2020;36:1823–33.
22. Serafini G, Sconfienza LM, Lacelli F, et al. Rotator cuff calcific tendonitis: short-term and 10-year outcomes after two-needle us-guided percutaneous treatment-nonrandomized controlled trial. Radiology 2009; 252(1):157–64.
23. de Witte PB, Kolk A, Overes F, et al. Rotator cuff calcific tendinitis: ultrasound-guided needling and lavage versus subacromial corticosteroids: five-year outcomes of a randomized controlled trial. Am J Sports Med 2017;45(14):3305–14.
24. Gärtners J, Simons B. Analysis of calcific deposits in calcifying tendinitis. Clin Orthop Relat Res 1990;254: 111–20.
25. Malghem J, Omoumi P, Lecouvet F, et al. Intraosseous migration of tendinous calcifications: cortical erosions, subcortical migration and extensive intramedullary diffusion, a SIMS series. Skeletal Radiol 2015;44(10):1403–12.
26. Resnick D. Gouty arthritis. In: Diagnosis of bone and joint disorders. 4th edition. Articular diseases, vol 1. Philadelphia (PA): WB Saunders; 2002. p. 1519–1559.
27. Dehlin M, Jacobsson L, Roddy E. Global epidemiology of gout: prevalence, incidence, treatment patterns and risk factors. Nat Rev Rheumatol 2020; 16(7):380–90.
28. Kuo CF, Grainge MJ, Zhang W, et al. Global epidemiology of gout: prevalence, incidence and risk factors. Nat Rev Rheumatol 2015;11(11):649–62.
29. Smith EU, Díaz-Torné C, Perez-Ruiz F, et al. Epidemiology of gout: an update. Best Pract Res Clin Rheumatol 2010;24(6):811–27.
30. Elfishawi MM, Zleik N, Kvrgic Z, et al. The rising incidence of gout and the increasing burden of comorbidities: a population-based study over 20 years. J Rheumatol 2018;45(4):574–9.
31. Rai SK, Aviña-Zubieta JA, McCormick N, et al. The rising prevalence and incidence of gout in British Columbia, Canada: Population-based trends from 2000 to 2012. Semin Arthritis Rheum 2017;46(4):451–6.
32. Zobbe K, Prieto-Alhambra D, Cordtz R, et al. Secular trends in the incidence and prevalence of gout in Denmark from 1995 to 2015: a nationwide register-based study. Rheumatology (Oxford) 2019;58(5):836–9.
33. Cea Soriano L, Rothenbacher D, Choi HK, et al. Contemporary epidemiology of gout in the UK general population. Arthritis Res Ther 2011;13(2):R39.
34. Chen-Xu M, Yokose C, Rai SK, et al. Contemporary Prevalence of Gout and Hyperuricemia in the United States and Decadal Trends: The National Health and Nutrition Examination Survey, 2007-2016. Arthritis Rheumatol 2019;71(6):991–9.
35. Girish G, Melville DM, Kaeley GS, et al. Imaging 2ppearances in gout. Arthritis 2013;2013:673401.
36. de Ávila Fernandes E, Sandim GB, Mitraud SA, et al. Sonographic description and classification of tendinous involvement in relation to tophi in chronic tophaceous gout. Insights Imaging 2010;1(3):143–8.
37. Yuan Y, Liu C, Xiang X, et al. Ultrasound scans and dual energy CT identify tendons as preferred anatomical location of MSU crystal depositions in gouty joints. Rheumatol Int 2018;38(5):801–11.
38. Weniger FG, Davison SP, Risin M, et al. Gouty flexor tenosynovitis of the digits: report of three cases. J Hand Surg Am 2003;28(4):669–72.
39. Gerster JC, Landry M, Rappoport G, et al. Enthesopathy and tendinopathy in gout: computed tomographic assessment. Ann Rheum Dis 1996;55(12):921–3.
40. Perez-Ruiz F, Castillo E, Chinchilla SP, et al. Clinical manifestations and diagnosis of gout. Rheum Dis Clin North Am 2014;40(2):193–206.
41. Lioté F, Lancrenon S, Lanz S, et al. GOSPEL: prospective survey of gout in France. Part I: design and patient characteristics (n = 1003). Joint Bone Spine 2012;79(5):464–70.
42. Schwabl C, Taljanovic M, Widmann G, et al. Ultrasonography and dual-energy computed tomography: impact for the detection of gouty deposits. Ultrasonography 2021;40(2):197–206.

43. Choi HK, Atkinson K, Karlson EW, et al. Purine-rich foods, dairy and protein intake, and the risk of gout in men. N Engl J Med 2004;350(11):1093–103.
44. Jacques T, Michelin P, Badr S, et al. Conventional radiology in crystal arthritis: Gout, calcium pyrophosphate deposition, and basic calcium phosphate crystals. Radiol Clin North Am 2017;55(5):967–84.
45. McQueen FM, Chhana A, Dalbeth N. Mechanisms of joint damage in gout: evidence from cellular and imaging studies. Nat Rev Rheumatol 2012;8(3):173–81.
46. Klauser AS, Gruber J. Response to: "Monosodium urate crystal deposition associated with the progress of radiographic grade at the sacroiliac joint in axial SpA: a dual-energy CT study. Arthritis Res Ther 2020;20(1):28.
47. Finkenstaedt T, Manoliou A, Toniolo M, et al. Gouty arthritis: the diagnostic and therapeutic impact of dual-energy CT. Eur Radiol 2016;26(11):3989–99.
48. Bongartz T, Glazebrook KN, Kavros SJ, et al. Dual-energy CT for the diagnosis of gout: an accuracy and diagnostic yield study. Ann Rheum Dis 2015;74(6):1072–7.
49. Richette P, Doherty M, Pascual E, et al. 2018 updated European League Against Rheumatism evidence-based recommendations for the diagnosis of gout. Ann Rheum Dis 2020;79(1):31–8.
50. Bloch C, Hermann G, Yu TF. A radiologic reevaluation of gout: a study of 2,000 patients. AJR Am J Roentgenol 1980;134(4):781–7.
51. Dhanda S, Jagmohan P, Quek ST. A re-look at an old disease: a multimodality review on gout. Clin Radiol 2011;66(10):984–92.
52. Taljanovic MS, Melville DM, Gimber LH, et al. High-Resolution US of Rheumatologic Diseases. Radiographics 2015;35(7):2026–48.
53. Filippucci E, Di Geso L, Grassi W. Tips and tricks to recognize microcrystalline arthritis. Rheumatology (Oxford) 2012;51(Suppl 7):vii18–21.
54. Bruyn GA, Iagnocco A, Naredo E, et al. OMERACT Definitions for ultrasonographic pathologies and elementary lesions of rheumatic disorders 15 Years On. J Rheumatol 2019;46(10):1388–93.
55. de Ávila Fernandes E, Kubota ES, Sandim GB, et al. Ultrasound features of tophi in chronic tophaceous gout. Skeletal Radiol 2011;40(3):309–15.
56. Klauser AS, Halpern EJ, Strobl S, et al. Gout of hand and wrist: the value of US as compared with DECT. Eur Radiol 2018;28(10):4174–81.
57. Poh YJ, Dalbeth N, Doyle A, et al. Magnetic resonance imaging bone edema is not a major feature of gout unless there is concomitant osteomyelitis: 10-year findings from a high-prevalence population. J Rheumatol 2011;38(11):2475–81.
58. Cimmino MA, Zampogna G, Parodi M, et al. MRI synovitis and bone lesions are common in acute gouty arthritis of the wrist even during the first attack. Ann Rheum Dis 2011;70(12):2238–9.
59. Dalbeth N, Doyle AJ. Imaging of gout: an overview. Best Pract Res Clin Rheumatol 2012;26(6):823–38.
60. Johnson TR, Krauss B, Sedlmair M, et al. Material differentiation by dual energy CT: initial experience. Eur Radiol 2007;17(6):1510–7.
61. Hu HJ, Liao MY, Xu LY. Clinical utility of dual-energy CT for gout diagnosis. Clin Imaging 2015;39(5):880–5.
62. Choi HK, Al-Arfaj AM, Eftekhari A, et al. Dual energy computed tomography in tophaceous gout. Ann Rheum Dis 2009;68(10):1609–12.
63. Glazebrook KN, Guimarães LS, Murthy NS, et al. Identification of intraarticular and periarticular uric acid crystals with dual-energy CT: initial evaluation. Radiology 2011;261(2):516–24.
64. Strobl S, Halpern EJ, Ellah MA, et al. Acute gouty knee arthritis: ultrasound findings compared with dual-energy CT findings. AJR Am J Roentgenol 2018;210(6):1323–9.
65. Teh J, McQueen F, Eshed I, et al. Advanced imaging in the diagnosis of gout and other crystal arthropathies. Semin Musculoskelet Radiol 2018;22(2):225–36.
66. Dalbeth N, Choi HK. Dual-energy computed tomography for gout diagnosis and management. Curr Rheumatol Rep 2013;15(1):301.
67. Wang P, Smith SE, Garg R, et al. Identification of monosodium urate crystal deposits in patients with asymptomatic hyperuricemia using dual-energy CT. RMD Open 2018;4(1):e000593.
68. Garner HW, Wessell DE. Gout: update on dual-energy computed tomography with emphasis on artifact identification. Curr Rheumatol Rep 2018;20(12):86.
69. Mallinson PI, Coupal T, Reisinger C, et al. Artifacts in dual-energy CT gout protocol: a review of 50 suspected cases with an artifact identification guide. AJR Am J Roentgenol 2014;203(1):W103–9.
70. Park EH, Yoo WH, Song YS, et al. Not all green is tophi: the importance of optimizing minimum attenuation and using a tin filter to minimize clumpy artifacts on foot and ankle dual-energy CT. AJR Am J Roentgenol 2020;214(6):1335–42.
71. Choi HK, Burns LC, Shojania K, et al. Dual energy CT in gout: a prospective validation study. Ann Rheum Dis 2012;71(9):1466–71.
72. Strobl S, Kremser C, Taljanovic M, et al. Impact of Dual-Energy CT postprocessing protocol for the detection of gouty arthritis and quantification of tophi in patients presenting with podagra: comparison with ultrasound. AJR Am J Roentgenol 2019;213(6):1315–23.
73. Klauser AS, Halpern EJ, Strobl S, et al. Dual-energy computed tomography detection of cardiovascular monosodium urate deposits in patients with gout. JAMA Cardiol 2019;4(10):1019–28.
74. Feuchtner GM, Plank F, Beyer C, et al. Monosodium urate crystal deposition in coronary artery plaque by 128-slice dual-energy computed tomography: an ex vivo phantom and in vivo study. J Comput Assist Tomogr 2021;45(6):856–62.